alpha-ketoglutarate regulates acid-base balance through an intra-renal paracrine mechanism

Natsuko Tokonami[1*], Luciana Morla[2*], Gabriel Centeno[1], David Mordasini[1], Suresh Krishna Ramakrishnan[2], Svetlana Nikolaeva[1,3], Carsten A. Wagner[5], Olivier Bonny[1,4] , Pascal Houillier[2#], Alain Doucet[2#] and Dmitri Firsov[1#]

[1] - Department of Pharmacology and Toxicology, University of Lausanne, Switzerland

[2] - UPMC Univ Paris 06, University Paris Descartes and INSERM UMRS 872 team 3, and CNRS ERL 7226, Centre de recherche des Cordeliers, Paris, France

[3] - Institute of Evolutionary Physiology and Biochemistry, St-Petersburg, Russia

[4] - Service of Nephrology, Department of Medicine, CHUV, Lausanne, Switzerland

[5] - Institute of Physiology, University of Zurich, Switzerland

* - these authors contributed equally to this work

- to whom correspondence should be addressed:

Dmitri Firsov Department of Pharmacology and Toxicology, University of Lausanne, 27 rue du Bugnon, 1005 Lausanne, Switzerland.

e-mail: dmitri.firsov@unil.ch, phone: ++41 21 6925406, fax: ++41 21 6925355

Alain Doucet ERL7226-UMRS872 Centre de Recherche des Cordeliers, 15, rue de l'Ecole de Médicine, 75270 Paris, France.

e-mail: alain.doucet@crc.jussieu.fr, phone: ++33 1 44275010, fax: ++33 1 44275119

Pascal Houillier Renal and Metabolic Diseases Unit, Georges Pompidou Hospital, Paris Descartes University, Cordeliers Research Center, 15, rue de l'Ecole de Médicine, 75270 Paris, France. e-mail: pascal.houillier@egp.aphp.fr, phone: ++33 1 56093972, Fax: ++33 1 56092675

The authors have declared that no conflict of interest exists.

Paracrine communication between different parts of the renal tubule is increasingly recognized as playing an important role in renal function. Previous studies have shown that changes in dietary acid-base load could reverse the direction of apical alpha-ketoglutarate (αKG) transport in the proximal tubule and Henle's loop from reabsorption (acid load) to secretion (base load). Here we show that the resulting changes in the luminal concentrations of αKG are sensed by the αKG receptor Oxgr1 expressed in the type B and non-A-non-B intercalated cells of the connecting tubule (CNT) and the cortical collecting duct (CCD). αKG (1mM) added to the tubular lumen strongly stimulated Cl^--dependent HCO_3^- secretion and electroneutral transepithelial NaCl reabsorption in microperfused CCD of wild-type mice but not *oxgr1*$^{-/-}$ mice. Analysis of alkali-loaded mice revealed a significantly reduced ability of *oxgr1*$^{-/-}$ mice to maintain acid-base balance. Collectively, these results demonstrated that Oxgr1 is involved in the adaptive regulation of HCO_3^- secretion and NaCl reabsorption in the CNT/CCD under acid-base stress and established αKG as a paracrine mediator involved in the functional coordination of the proximal and the distal parts of the renal tubule.

INTRODUCTION

Alpha-ketoglutarate (αKG) is an intermediate of the citric acid cycle (TCA), an important anaplerotic substrate and a co-factor in a variety of enzymatic reactions. In addition to its direct effects on metabolic pathways, αKG was identified as a natural ligand to a G protein-coupled receptor (GPCR), namely GPR99 or 2-oxoglutarate receptor 1 (Oxgr1) (1). Oxgr1 belongs to a cluster of so-called "metabolic" GPCRs, which also includes receptors for succinate (GPR91), lactate (GPR81), 3-hydroxy-octanate (GPR109B), nucleotides (P2Y), fatty acids (FFAR), lipids (P2RY, CysLT, Oxer1, etc.), phospholipids (PAF), protease-activated receptors (PAR) and several orphan receptors (2). He et al, have shown that Oxgr1 is a Gq-coupled GPCR that is predominantly expressed in distal tubules in the kidney (1). However, the functional role of Oxgr1 has not been studied.

Previous studies in rats demonstrated that renal handling of αKG changes significantly in response to changes in acid-base status. αKG is freely filtered in the glomerulus and, under normal conditions, actively reabsorbed in the proximal tubule and Henle's loop. Acid load further stimulates αKG reabsorption, thus resulting in drop in urinary output of αKG. Under base loading conditions, the blood concentration of αKG rises and net αKG reabsorption in the proximal tubule and Henle's loop is converted to net αKG secretion in the same nephron segments (3-5). This results in a significant increase in the urinary excretion of αKG. It has been proposed that excretion of αKG and other organic anions (e.g. citrate) in the urine represents the loss of "potential HCO_3^-" which provides the advantage of minimizing bicarbonaturia under alkali load (6). The latter is important because it allows the excretion of base at a lower urinary pH, thereby diminishing the risk of nephrolithiasis due to the formation of calcium-phosphate precipitates (αKG: pKa_1(1.9), pKa_2(4.4); bicarbonate: pKa_1(6.1); HPO_4^{2-}: pKa_2(6.7-6.8) in the

urine (5, 7). Collectively, these results demonstrated that acid-base status is a major factor determining blood levels of αKG and the rate of αKG excretion into urine. Importantly, Ferrier et al. have shown that there is no net transport of αKG beyond the beginning of the distal tubule accessible to micropuncture (3). This indicated that variations in the urinary αKG concentration are directly proportional to the variations in the luminal levels of αKG in the CNT/CCD, where Oxgr1 is expressed (see below). Taken together, these data led us to hypothesize that Oxgr1 could be involved in the apical and/or basolateral sensing of acid-base status through the sensing of αKG concentrations in the tubular fluid and/or in the blood.

Testing this hypothesis revealed that luminal Oxgr1 regulates Cl^--dependent HCO_3^- secretion and electroneutral transepithelial NaCl reabsorption in the type B and non-A-non-B intercalated cells of the CNT/CCD. We show that this regulation is functionally important since mice devoid of Oxgr1 exhibit a reduced capacity to maintain acid-base equilibrium under base load conditions. We hypothesize that Oxgr1-mediated NaCl reabsorption in the type B and non-A-non-B intercalated cells is required to compensate for the increased or decreased activity of sodium-hydrogen exchanger 3 (NHE3) in the proximal tubule and Henle's loop under acid or base loading conditions, respectively. Collectively, our results show for the first time that the kidney possesses a paracrine mechanism involved in the control of acid-base balance. In this mechanism, αKG acts as a paracrine mediator between the proximal and the distal parts of the renal tubule.

RESULTS

To identify renal cell types expressing Oxgr1 we used mice whose *oxgr1* gene was deleted and replaced with a reporter gene encoding beta-galactosidase (*LacZ*). X-gal staining on kidney sections demonstrated patchy expression of Oxgr1 in cortical tubules (Supplementary Figures 1A and 1B). Co-staining with a panel of cell-type specific markers revealed that Oxgr1 co-localizes at the cellular level with pendrin, a Cl^-/HCO_3^- exchanger that is exclusively expressed at the apical membrane of the type B and non-A-non-B intercalated cells of the connecting tubule (CNT) and the cortical collecting duct (CCD) (Figure 1A-1F). This specific cellular localization was validated by the absence of co-staining with parvalbumin (a marker of the early distal convoluted tubule, Supplementary Figures 1C-1E), the sodium chloride co-transporter (NCC) (a marker of the early and late distal convoluted tubule, Supplementary Figures 1F-1H), the beta subunit of the amiloride-sensitive sodium channel (ENaC) (a marker of the late distal convoluted tubule and the principal cells of the CNT and the CCD, Supplementary Figures 1I-1N), aquaporin-2 (a marker of principal cells of the CNT and the CCD, Supplementary Figures 1O-1T) and anion exchanger 1 (AE1) (a marker of type A intercalated cells of the CNT and the CCD, Supplementary Figures 1U-1Z). The type B and non-A-non-B intercalated cells in the CNT and the CCD are involved in the control of systemic acid-base homeostasis, extracellular fluid volume and blood pressure (reviewed in (8-10)). Pendrin participates in these functions by controlling HCO_3^- secretion, electroneutral Na^+-Cl^- reabsorption (upon functional coupling with Na^+-driven Cl^-/HCO_3^- exchanger NDCBE (Slc4a8) (11), and by regulating Na^+ reabsorption in the adjacent principal cells (12).

To examine whether αKG is capable of regulating apical Cl^-/HCO_3^- exchange activity we determined the activity of pendrin in intercalated cells of isolated CCDs by measuring the rate of intracellular acidification induced by the addition of luminal Cl^- (forward activity) or

alkalinization following Cl^- removal (reverse activity). As shown in Figure 2A, addition of 1 mM αKG to the luminal perfusion solution increased the rate of Cl^-/HCO_3^- exchange in intercalated cells of CCDs from *oxgr1*$^{+/+}$ but not *oxgr1*$^{-/-}$ mice, although the exchanger displayed a similar baseline activity in the two mouse strains. A representative trace depicting the effect of 1mM αKG on intracellular pH in intercalated cells of CCD is shown in Supplementary Figure 2. Western blot analysis demonstrated that pendrin protein abundance was not different between *oxgr1*$^{+/+}$ and *oxgr1*$^{-/-}$ mice (Supplementary Figures 3A and 3D).

Next, we evaluated whether stimulation of luminal Cl^-/HCO_3^- exchange was associated with increased electroneutral NaCl reabsorption. Using *in vitro* microperfusion of CCDs from *oxgr1*$^{+/+}$ mice, we found that addition of 1 mM αKG to the tubular lumen induced an equimolar reabsorption of Na^+ and Cl^- whereas basolateral αKG had no effect (Figure 2B). αKG-induced reabsorption of NaCl was markedly reduced by hydrochlorothiazide, an inhibitor of the electroneutral component of sodium reabsorption in the CCD. Interestingly, CCDs from *oxgr1*$^{-/-}$ mice displayed baseline Na^+ but not Cl^- transport which was abolished by the ENaC inhibitor amiloride. Luminal addition of αKG did not increase electroneutral NaCl reabsorption in CCD from *oxgr1*$^{-/-}$ mice but abolished ENaC-mediated Na^+ reabsorption (Figure 2B). Western blot analysis revealed an increase in abundance of αENaC (*oxgr1*$^{+/+}$: 100 ± 7 (SEM, n=6) vs. *oxgr1*$^{-/-}$: 136 ± 5 (SEM, n=6), arbitrary units, p=0.003, Supplementary Figures 3B and 3D) but not in abundance of βENaC subunit (Supplementary Figures 3C and 3D).

Altogether, these results demonstrate that activation of luminal Oxgr1 by αKG stimulates pendrin activity and electroneutral reabsorption of NaCl by type B and non-A-non-B intercalated cells. They also suggest that ENaC activity is increased in the knockout mice and that luminal αKG may inhibit ENaC independently of Oxgr1.

Next, we assessed whether challenges of acid-base or NaCl homeostasis cause changes in the luminal levels of αKG in the CNT/CCD or in the systemic circulation in mice. Wild-type C57BL/6 mice housed in metabolic cages were challenged with an oral acid, alkali or NaCl load (0.3 M NH_4Cl, 0.28 M $NaHCO_3$ or 0.28 M NaCl in drinking water, respectively) for 1, 3, 5 or 7 days. αKG levels were measured in 24-hour urine samples or in serum samples collected at the end of the experiment. As shown in Figure 3A and Supplementary Figure 4A, the acid load induced a striking decrease in urinary [αKG]/[creatinine] ratios and urinary αKG concentrations, respectively, whereas base load resulted in an opposite pattern with a significant increase in urinary αKG levels. The changes in urinary αKG levels were parallel to changes in urinary pH (supplementary Figure 4B). At the same time, addition of NaCl to drinking water did not produce any effect on urinary αKG levels (Figure 3A and Supplementary Figure 4A). Importantly, none of the dietary supplements had a significant effect on plasma αKG concentration even though there was a tendency for increased αKG concentration in mice loaded with $NaHCO_3$ (Figure 3B). To test whether base load can produce more rapid (<24 hours) effects on urinary αKG levels and to assess the threshold dose of base capable to increase αKG concentrations in urine, mice were gavaged with 400 μl solution containing various concentrations of $NaHCO_3$. Spot urine was collected 3 hours after gavage. As control groups, mice gavaged with 400 μl of either water or 0.56 M NaCl were used. As shown in Figure 3C, water or 0.56 M NaCl-gavaged mice excreted similar amounts of αKG in the urine. Base load induced a significant increase in both urinary pH and αKG/creatinine ratios when compared with water or NaCl controls (Figure 3C). Importantly, these changes reached statistical significance already at low doses of $NaHCO_3$ (22.4 μmol $NaHCO_3$ for αKG/creatinine ratio and 44.8 μmol $NaHCO_3$ for urinary pH). Collectively, these

results demonstrated that the challenge of mice with acid/base but not NaCl load can produce rapid and significant effects on urinary αKG levels.

To test whether deficiency of Oxgr1 could affect acid-base equilibrium, we analyzed urine and blood samples of wild-type and *oxgr1*$^{-/-}$ mice. As shown in Table 1, *oxgr1*$^{-/-}$ mice fed standard diet had a small but statistically significant decrease in urine pH and a statistically significant increase in urinary titratable acid and αKG levels. These results suggested that the acid-base equilibrium might be disturbed in *oxgr1*$^{-/-}$ mice. However, blood chemistry parameters were not different between wild-type and *oxgr1*$^{-/-}$ mice (Table 1). Thus, we tested the role of Oxgr1 in the condition of experimentally induced alkalosis. As shown in Table 1, both wild-type and *oxgr1*$^{-/-}$ mice given a $NaHCO_3$-rich diet for 3 days (see Methods) developed a metabolic alkalosis with plasma HCO_3^- levels raised above 30 mM. However, the increase in plasma HCO_3^- levels was significantly higher in *oxgr1*$^{-/-}$ mice. **Tubular handling of bicarbonate under alkali load was examined in a separate experiment by assessing its fractional excretion (FE_{HCO3}). As shown in Table 1, the FE_{HCO3} was more than two fold lower in *oxgr1*$^{-/-}$ mice compared to wild-type mice, thus suggesting an inappropriate renal/tubular response in *oxgr1*$^{-/-}$ mice to the alkali load. Collectively,** these results indicated that renal mechanisms responsible for maintaining acid-base equilibrium upon alkali load are impaired in *oxgr1*$^{-/-}$ mice. The fact that plasma Cl^- concentration was significantly lower in *oxgr1*$^{-/-}$ mice (Table 1) suggested that a decrease in the HCO_3^-/Cl^- exchange activity via pendrin is involved in this impairment.

DISCUSSION

Paracrine signaling plays an important role in renal function. For instance, the tubuloglomerular feedback response which is mediated by a multitude of paracrine molecules (ATP, adenosine,

prostaglandin E2 and nitric oxide), is critically involved in the regulation of glomerular filtration rate (GFR) (reviewed in (13)). In the present study we show for the first time that maintaining systemic acid-base balance requires paracrine communication between the proximal and the distal parts of the renal tubule. We demonstrate that αKG acts in a paracrine manner on type B and non-A-non-B intercalated cells of the CNT/CCD stimulating HCO_3^- secretion and NaCl reabsorption. These effects are induced by apical but not basolateral application of αKG and are mediated by Oxgr1, a GPCR that is specifically expressed in type B and non-A-non-B intercalated cells. Importantly, our estimations suggest that luminal levels of αKG in the CNT/CCD vary within the range of αKG concentrations that have been shown to activate Oxgr1 *in vitro* (EC50 ~70 μM (1)). Indeed, considering that under our experimental condition urine is concentrated approximately 10-20 times between the lumen of the CNT/CCD and the final urine, one can estimate the range of αKG concentration at the site of Oxgr1 expression as several hundreds nanomolar under acid load, as one hundred to several hundreds micromolar under standard diet and as one to several millimolar under base load (e.g. the concentration of αKG in the final urine of mice given 0.3 M NH_4Cl in drinking water for 2 days is: 3.53 ± 2.10 μM (n=6, SD), the concentration of αKG in the final urine of mice given tap water is 2.03 ± 0.67 mM (n=6, SD) and the concentration of αKG in the final urine of mice given 0.28 M $NaHCO_3$ in drinking water for 2 days is 36.43 ± 8.16 mM (n=6, SD), see Supplementary Figure **4**A). Another piece of evidence supporting the functional relevance of this paracrine signaling is the finding that significant changes in urinary levels of αKG occur rapidly (less than 3 hours) in response to acid/base stress and that these changes can be induced by low, physiologically relevant doses of acid or base (e.g. the dose of 22.4 μmol $NaHCO_3$, which produced a significant effect on the urinary αKG levels in gavage experiments is significantly lower than the amount of HCO_3^-

produced by the metabolism of 1 g of the 24% protein-containing standard diet used in this study). This suggests that the activation level of this paracrine mechanism can be modulated by the diurnal variations in the dietary acid-base load and/or by the variations in body's metabolic production of acid and base.

We propose that αKG/Oxgr1 paracrine signaling is involved in maintenance of acid-base balance at least in two ways. Firstly, this paracrine mechanism controls pendrin activity thereby exerting a direct effect on the acid-base balance. The rapid onset of pendrin activation by αKG/Oxgr1 (within 20 min) suggests that this regulation is transcriptionally independent. Together with the results showing rapid changes in urinary αKG levels under acute acid-base stress, these observations support the hypothesis that the αKG-Oxgr1-pendrin axis is involved in the dynamic fine-tuning of bicarbonate secretion by type B and non-A-non-B intercalated cells. Secondly, we hypothesize that αKG/Oxgr1signaling may be involved in the compensatory response to the acid-base stress-induced changes in NaCl reabsorption through the sodium-hydrogen exchanger 3 (NHE3) in the proximal tubule and Henle's loop. Indeed, it was demonstrated that acute acid or base loading induces an increase or decrease in the NHE3 activity, respectively (reviewed in (14). Because NHE3 is functionally coupled to a Cl^-/ anion exchange, these changes result not only in the increased or decreased bicarbonate reabsorption but also in the increased or decreased net NaCl reabsorption in the proximal tubule, respectively. Thus, by decreasing or increasing NaCl reabsorption in the type B and non-A-non-B intercalated cells under acid or base loading, respectively, the αKG/Oxgr1 signaling participates in maintaining NaCl homeostasis and, indirectly, in acid-base balance. This model is depicted in the Supplementary Figure 5. To what extent this paracrine mechanism operates similarly/differentially between type B and type non-A/non-B intercalated cells or between CNT

and CCD (which contain different ratios of these cell types) remains to be established in future studies. The idea that the αKG/Oxgr1 pathway is involved in sodium balance is supported by the fact that *oxgr1*$^{-/-}$ mice exhibit an increased functional activity of ENaC correlating with the increased protein abundance of αENaC subunit. The mechanism of these adaptive changes remains unknown, but our data indicate that they occur without changes in plasma aldosterone levels.

Besides its Oxgr1-mediated stimulatory action on NaCl reabsorption in intercalated cells, αKG also inhibits amiloride-sensitive Na^+ reabsorption in principal cells independently of Oxgr1 activation. This metabolic effect of αKG may be related to increased ATP production and inhibition of amiloride-sensitive epithelial sodium channel (ENaC) via autocrine activation of P2Y2 receptors (15). Receptor-dependent and -independent effects of αKG on intercalated and principal cells both converge to compensate alkalosis-induced decrease in proximal tubule reabsorption of NaCl by favouring NaCl reabsorption over Na^+/K^+ exchange along the CNT/CCD.

Our finding that αKG serves as a paracrine mediator in regulating acid-base balance adds to the accumulating evidence for the regulatory homeostatic role of organic anions excreted in urine. It has been long recognized that citrate, the major intermediate of TCA cycle in the urine, has a dual role in maintaining acid-base balance and in the chelation of calcium ions, thereby preventing calcium stone formation (reviewed in (16)). Peti-Peterdi and colleagues have recently demonstrated the role of luminal succinate in GPR91-mediated regulation of renin secretion (17, 18). Today, citrate supplementation is widely used in the prevention of nephrolithiasis and GPR91 is recognized as a potential target in treatment of diabetic nephropathy. Our results and the fact that Oxgr1 expression is almost exclusively restricted to the kidney suggest that Oxgr1

could represent an interesting therapeutic opportunity for treatment of acid-base disorders, or in the treatment of tubular disorders associated with kidney stones formation. The second tissue that exhibits a high level of Oxgr1 expression is the testis and epididymis (19). Whether Oxgr1 is involved in the homeostasis of epididymal fluid and male fertility needs to be addressed by future investigation.

Experimental Procedures

Animals A colony of *oxgr1*$^{-/-}$ mice (C57BL/6J background) was established from breeding pairs of *oxgr1*$^{+/-}$ heterozygous developed by Velocigene and obtained from the Knock-Out Mouse Project (KOMP) repository. Male mice weighing 25-30 g and 8 weeks of age were used in all experiments. The animals were maintained on the standard laboratory chow diet (KLIBA NAFAG diet 3800). The $NaHCO_3$-rich and standard jelly diets were prepared as follows: 6 ml of 0.7 M $NaHCO_3$ or 6 ml of water were mixed with 0.2 ml agar-agar solution and briefly boiled. The resulting solution was cooled down to 40°C and mixed with 5g of the standard lab chow in the form of powder. The final mixture was stored at 4°C for a maximum of 3 days. The mice received 11 g of the jelly food per day. All experiments with animals were performed in accordance with the Swiss guidelines for animal care.

Antibodies The antibodies against NCC, aquaporin-2, αENaC, βENaC, AE1 and pendrin have been used as previously described (20, 21). Anti-parvalbumin antibody was from Swant (Switzerland). Anti-beta-galactosidase antibody was from Abcam. Anti-actin antibody was from Sigma. We have tested several commercially available anti-Oxgr1 antibodies (2-oxoglutarate receptor 1 antibody 18-461-10700 from GenWay, anti-Oxgr1 antibody ab67351 from Abcam and anti-Oxgr1 antibody LS-A1865 from LifespanBiosciences), however, none of them have shown

specific results. Immunohistochemistry and X-gal staining protocols are available in the Supplementary Methods.

Metabolic cages Mice were housed in individual metabolic cages (Tecniplast, Italy). Urine collection was performed after a 3-day adaptation period. Urine osmolality, pH and ionic composition were analyzed as previously described (22).

Blood sample analysis In experiments with alkali load, blood pH and blood gases were analyzed in blood samples collected from the retro-orbital sinus under isoflurane anesthesia. In mice fed a normal diet, blood was collected through a catheter implanted into the left carotid artery 4 hours before blood collection.

αKG measurement Urine and plasma αKG was measured using an Alpha-Ketoglutarate Assay Kit from BioVision.

Ion flux in isolated CCD. CCDs from WT and *oxgr1*$^{-/-}$ mice were microdissected from corticomedullary rays and microperfused under symmetrical conditions. The bath and perfusate contained (in mM): 118 NaCl, 23 $NaHCO_3$, 1.2 $MgSO_4$, 2 K_2HPO_4, 2 calcium lactate, 1 Na-citrate, 5.5 glucose, 12 creatinine, pH 7.4 (bath continuously gassed with 95% O_2/5% CO_2) at 37°C. Measurements were conducted during the first 90 minutes of perfusion. Hydrochlorothiazide and amiloride were added to the perfusate at a final concentration of 10^{-4} M and 10^{-5} M, respectively. Collections from 4 periods of 15 minutes were performed in which 30–35 nl of fluid was collected. The collection volume was determined under water-saturated mineral oil with calibrated volumetric pipettes. Concentrations of Na^+ and creatinine were determined by HPLC using 26 nl of collected fluid. Concentration of Cl- was measured by microcoulometry on 2-3 nl of collected fluid. For each collection, the ion flux of sodium (J_X) was calculated per unit length of tubule: $J_X = [([X]_p \times V_p) - ([X]_c \times V_c)] / (L \times t)$ where $[X]_p$ and $[X]_c$ are the concentrations of X in the perfusate and collection respectively, V_p and V_c are the

perfusion and collection rates respectively, L is the tubule length and t is the collection time. V_p was calculated as: $V_p = V_c \times [creat]_c / [creat]_p$ where $[creat]_c$ and $[creat]_p$ are the concentrations of creatinine in the collection and perfusate, respectively. For each tubule, ion fluxes were calculated as the mean of the four collection periods.

Apical Cl^-/HCO_3^- exchange activity in CCD intercalated cells. The activity of pendrin was determined by measuring the rate of intracellular alkalinization in type B and non-A-non-B intercalated cells following removal of luminal chloride as previously described (see Supplementary Methods for cell type identification). Our setup allowed a smooth and complete exchange of the luminal fluid within 3-4 s. Briefly, CCDs were dissected and microperfused *in vitro* as described above. Intracellular pH was assessed with imaging-based, dual excitation-wavelength fluorescence microscopy using 2',7'-Bis- (2-Carboxyethyl)-5- (And-6)-carboxyfluorescein (BCECF, Molecular probes). Intracellular dye was excited alternatively at 440 and 500 nm every 2 seconds with a light-emitting diode (Optoled, Cairn Research, Faversham, UK). Emitted light was collected through a dichroïc mirror, passed through a 530 nm filter and focused onto a EM-CCD camera (iXon, Andor Technology, Belfast, Ireland) connected to a computer. The measured light intensities were digitized with 14-bit precision (16384 grey level scale) for further analysis. For each tubule, 3-4 intercalated cells were analyzed and the mean grey level was measured with the Andor IQ software (Andor Technology, Belfast, Ireland). Background fluorescence was subtracted from fluorescence intensity to obtain intensity of intracellular fluorescence. Intracellular dye was calibrated at the end of each experiment using the high $[K^+]$-nigericin technique. CCDs were initially perfused with a Cl^--containing solution (in mM: 119 NMDG-Cl, 23 NMDG-HCO_3, 2 K_2HPO_4, 1.5 $CaCl_2$, 1.2 $MgSO_4$, 10 HEPES, and 5.5 D-glucose) and then switched to a Cl^--free solution (in mM: 119 NMDG-gluconate, 23 NMDG-

HCO_3, 2 K_2HPO_4, 7.5 Ca-gluconate, 1.2 $MgSO_4$, 10 HEPES, and 5.5 D-glucose). All solutions were adjusted to pH 7.40 and continuously bubbled with 95% O_2/5% CO_2.

Statistics. Data are presented as mean ± SEM or, as mean ± SD, as indicated in the corresponding figure legends. The tests used include the 2-tailed, unpaired *t*-test and the one-way ANOVA. All *P* values are indicated in the figure legends. A *P* value less than 0.05 was considered significant.

Study approval Animal studies were approved by the Veterinary Service of the Canton de Vaud, Switzerland.

ACKNOWLEDGMENTS We thank Dr. Dominique Eladari for helpful discussions and advice. We thank J. Loffing (University of Zurich) for providing antibodies against NCC, aquaporin-2, αENaC and βENaC. This work was supported by the Swiss National Science Foundation research grants 31003A-132496 (to D.F.) and 31003A-138143 (to C.A.W.) and by a grant from the Novartis Foundation (to D.F.)

FIGURE LEGENDS

Figure 1. Oxgr1 is expressed in type-B and non-A-non-B intercalated cells of the connecting tubule (CNT) and the cortical collecting duct (CCD). **A**. Immunostaining (green) with anti-β-galactosidase antibody shows that Oxgr1 is expressed in a subset of cells in the renal cortex. **B.** Immunolocalization of pendrin (red) in the apical membrane of type-B and non-A-non-B intercalated cells. **C.** Co-immunostaining with anti-β-galactosidase and anti-pendrin antibodies demonstrates that Oxgr1 and pendrin are expressed in the same cells. **D**, **E** and **F** are high magnification images for **A**, **B** and **C**, respectively. Nuclei (DNA) are stained with DAPI (blue, **C** and **F**). Scale bars: 50μm.

Figure 2. Activation of Oxgr1 stimulates pendrin and induces NaCl reabsorption in CCD. **A**. Apical Cl^-/HCO_3^- exchange activity was measured in intercalated cells from CCDs isolated from wild type (WT) and *oxgr1*$^{-/-}$ mice in the absence or the presence of 1 mM αKG in the luminal fluid. The exchanger activity was determined either in the forward (Cl^- addition induces intracellular acidification) or reverse direction (Cl^- removal induces intracellular alcalinization). Values are means ± SEM from 3 CCDs, the exchange activity being measured on at least 3 cells per CCD. Statistical significance as compared to controls (absence of αKG) by Student's t test **B.** Na^+ and Cl^- reabsorption fluxes (J_{Na+} and J_{Cl-} respectively) measured in *in vitro* microperfused CCDs from wild type (WT) and *oxgr1*$^{-/-}$ mice were determined in the absence or presence of 1 mM αKG in the luminal (L) or peritubular solution (B). Some CCDs were pre-treated with 100 μM hydrochlorothiazide (HCTZ) or 10 μM amiloride (Am). Note that in absence of αKG, CCDs fron WT mice displayed no NaCl transport whereas those from *oxgr1*$^{-/-}$ mice showed amiloride-sensitive Na^+ reabsorption which was inhibited upon addition of αKG. Values are means ± SEM

from 4-6 CCDs. Statistical significance as compared to controls (absence of αKG) by variance analysis (ANOVA).

Figure 3. Effects of a dietary load of acid, base or NaCl on urinary and plasma levels of αKG. **A.** Analysis of [αKG]/[creatinine] ratios in urines collected from wild-type mice housed individually in metabolic cages. The 24-hour urine was collected from four groups of mice (6 mice/group): a control group receiving tap-water (green) and groups supplemented with acid (0.3 M NH_4Cl, blue), base (0.28 M $NaHCO_3$, red) or salt (0.28 M NaCl, purple) in drinking water. Values are means ± SEM. ***, significantly different (P<0.005) compared to 0.28 M NaCl group; ###, significantly different (P<0.005) compared to H_2O group; Student's t-test. **B.** Analysis of plasma αKG concentrations in wild-type mice loaded for 7 days with acid (0.3 M NH_4Cl, blue), base (0.28 M $NaHCO_3$, red) or salt (0.28 M NaCl, purple) in drinking water. Mice in control group received tap-water (green) Values are means ± SD (n=6-9), ns - not significant; Student's t-test. **C.** Analysis of urinary [αKG]/[creatinine] ratios (red bars) and urinary pH (grey bars) in spot urines of wild-type mice gavaged with 400 μl of tap-water, 400 μl of 0.56 M NaCl, or 400 μl of $NaHCO_3$ at different concentrations (0.0056 M, 0.056 M, 0.112 M, 0.224 M and 0.448 M). The urine was collected 3 hours after gavage. Values are means ± SEM. ***, significantly different (P<0.005) compared to water group; ###, significantly different (P<0.005) compared to 0.56 M NaCl group; ##, significantly different (P<0.01) compared to 0.56 M NaCl group. Statistical significance as compared to controls by variance analysis (ANOVA).

1. He, W., Miao, F.J., Lin, D.C., Schwandner, R.T., Wang, Z., Gao, J., Chen, J.L., Tian, H., and Ling, L. 2004. Citric acid cycle intermediates as ligands for orphan G-protein-coupled receptors. *Nature* 429:188-193.
2. Tikhonova, I.G., Sum, C.S., Neumann, S., Thomas, C.J., Raaka, B.M., Costanzi, S., and Gershengorn, M.C. 2007. Bidirectional, iterative approach to the structural delineation of the functional "chemoprint" in GPR40 for agonist recognition. *J Med Chem* 50:2981-2989.

3. Ferrier, B., Martin, M., and Baverel, G. 1985. Reabsorption and secretion of alpha-ketoglutarate along the rat nephron: a micropuncture study. *Am J Physiol* 248:F404-412.
4. Martin, M., Ferrier, B., and Baverel, G. 1989. Transport and utilization of alpha-ketoglutarate by the rat kidney in vivo. *Pflugers Arch* 413:217-224.
5. Cheema-Dhadli, S., Lin, S.H., and Halperin, M.L. 2002. Mechanisms used to dispose of progressively increasing alkali load in rats. *Am J Physiol Renal Physiol* 282:F1049-1055.
6. Packer, R.K., Curry, C.A., and Brown, K.M. 1995. Urinary organic anion excretion in response to dietary acid and base loading. *J Am Soc Nephrol* 5:1624-1629.
7. Schwartz, W.B., Bank, N., and Cutler, R.W. 1959. The influence of urinary ionic strength on phosphate pK2' and the determination of titratable acid. *J Clin Invest* 38:347-356.
8. Wagner, C.A., Mohebbi, N., Capasso, G., and Geibel, J.P. 2011. The anion exchanger pendrin (SLC26A4) and renal acid-base homeostasis. *Cell Physiol Biochem* 28:497-504.
9. Wall, S.M., and Pech, V. 2008. The interaction of pendrin and the epithelial sodium channel in blood pressure regulation. *Curr Opin Nephrol Hypertens* 17:18-24.
10. Eladari, D., Chambrey, R., and Peti-Peterdi, J. 2012. A new look at electrolyte transport in the distal tubule. *Annu Rev Physiol* 74:325-349.
11. Leviel, F., Hubner, C.A., Houillier, P., Morla, L., El Moghrabi, S., Brideau, G., Hassan, H., Parker, M.D., Kurth, I., Kougioumtzes, A., et al. 2010. The Na+-dependent chloride-bicarbonate exchanger SLC4A8 mediates an electroneutral Na+ reabsorption process in the renal cortical collecting ducts of mice. *J Clin Invest* 120:1627-1635.
12. Kim, Y.H., Pech, V., Spencer, K.B., Beierwaltes, W.H., Everett, L.A., Green, E.D., Shin, W., Verlander, J.W., Sutliff, R.L., and Wall, S.M. 2007. Reduced ENaC protein abundance contributes to the lower blood pressure observed in pendrin-null mice. *Am J Physiol Renal Physiol* 293:F1314-1324.
13. Schnermann, J., and Levine, D.Z. 2003. Paracrine factors in tubuloglomerular feedback: adenosine, ATP, and nitric oxide. *Annu Rev Physiol* 65:501-529.
14. Bobulescu, I.A., and Moe, O.W. 2009. Luminal Na(+)/H (+) exchange in the proximal tubule. *Pflugers Arch* 458:5-21.
15. Vallon, V., and Rieg, T. 2011. Regulation of renal NaCl and water transport by the ATP/UTP/P2Y2 receptor system. *Am J Physiol Renal Physiol* 301:F463-475.
16. Moe, O.W., and Preisig, P.A. 2006. Dual role of citrate in mammalian urine. *Curr Opin Nephrol Hypertens* 15:419-424.
17. Toma, I., Kang, J.J., Sipos, A., Vargas, S., Bansal, E., Hanner, F., Meer, E., and Peti-Peterdi, J. 2008. Succinate receptor GPR91 provides a direct link between high glucose levels and renin release in murine and rabbit kidney. *J Clin Invest* 118:2526-2534.
18. Vargas, S.L., Toma, I., Kang, J.J., Meer, E.J., and Peti-Peterdi, J. 2009. Activation of the succinate receptor GPR91 in macula densa cells causes renin release. *J Am Soc Nephrol* 20:1002-1011.
19. Regard, J.B., Sato, I.T., and Coughlin, S.R. 2008. Anatomical profiling of G protein-coupled receptor expression. *Cell* 135:561-571.
20. Wagner, C.A., Loffing-Cueni, D., Yan, Q., Schulz, N., Fakitsas, P., Carrel, M., Wang, T., Verrey, F., Geibel, J.P., Giebisch, G., et al. 2008. Mouse model of type II Bartter's syndrome. II. Altered expression of renal sodium- and water-transporting proteins. *Am J Physiol Renal Physiol* 294:F1373-1380.
21. Loffing, J., Vallon, V., Loffing-Cueni, D., Aregger, F., Richter, K., Pietri, L., Bloch-Faure, M., Hoenderop, J.G., Shull, G.E., Meneton, P., et al. 2004. Altered renal distal tubule structure and renal Na(+) and Ca(2+) handling in a mouse model for Gitelman's syndrome. *J Am Soc Nephrol* 15:2276-2288.
22. Nikolaeva, S., Pradervand, S., Centeno, G., Zavadova, V., Tokonami, N., Maillard, M., Bonny, O., and Firsov, D. 2012. The circadian clock modulates renal sodium handling. *J Am Soc Nephrol* 23:1019-1026.

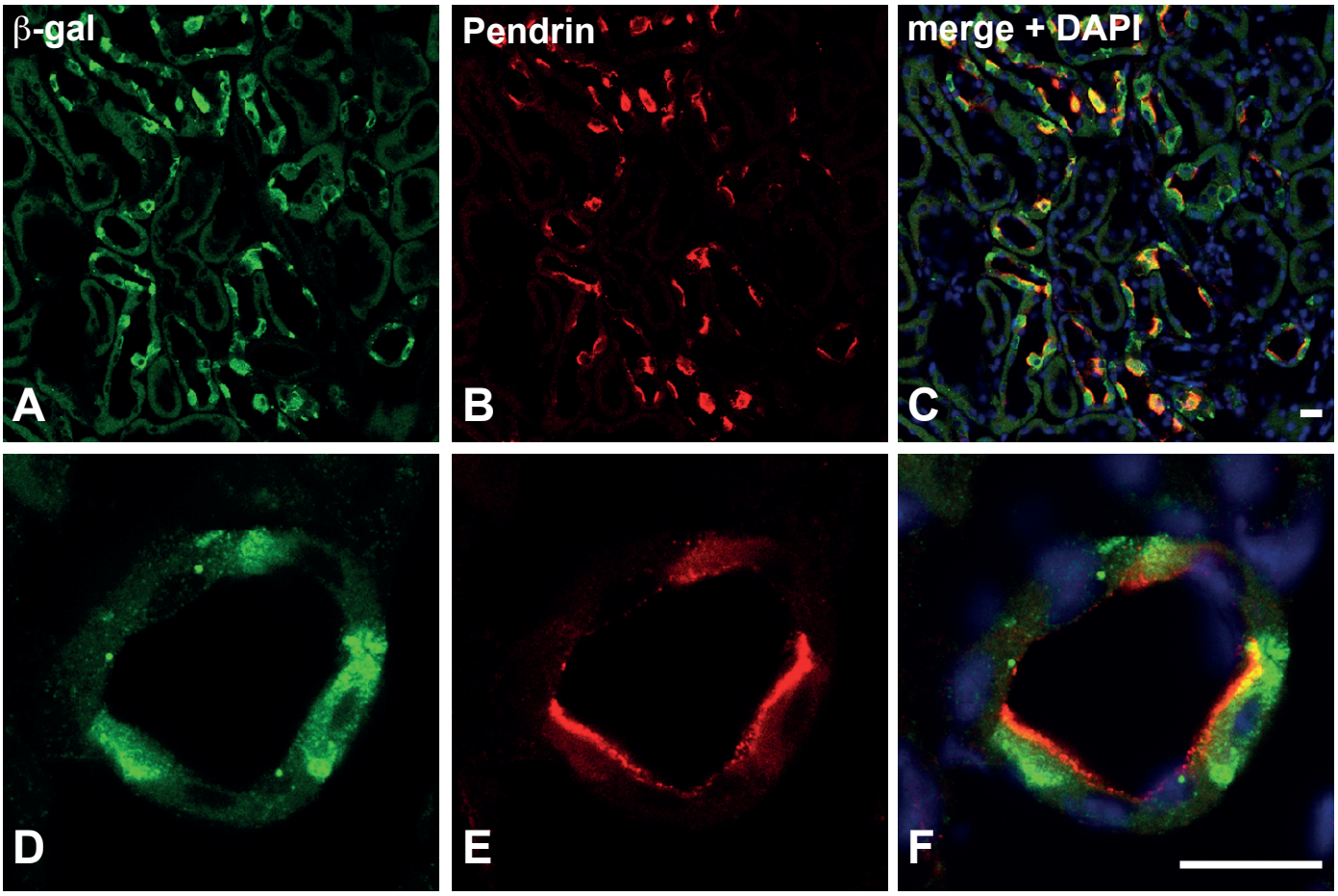

Figure 1. Tokonami et al.

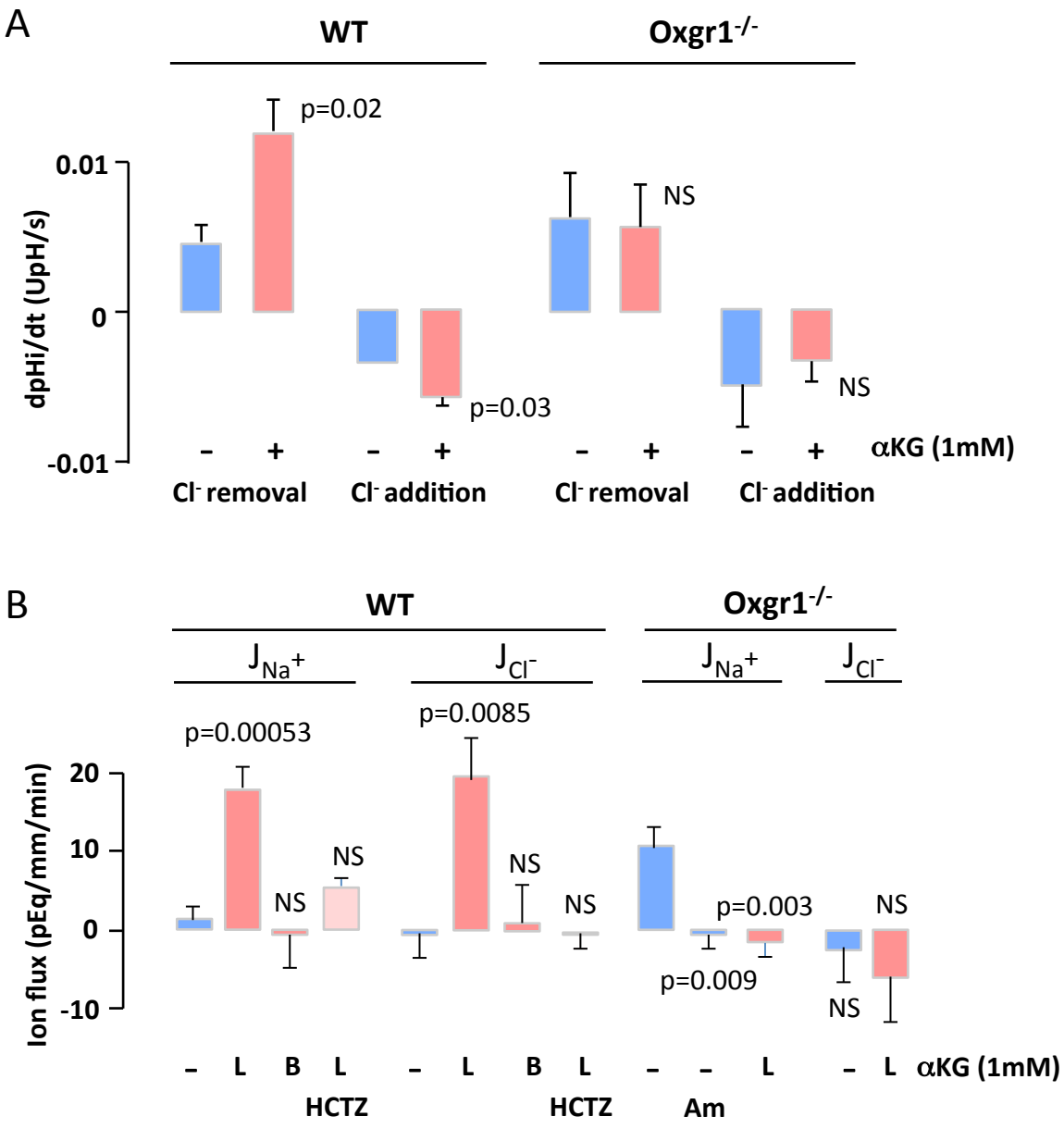

Figure 2. Tokonami et al.

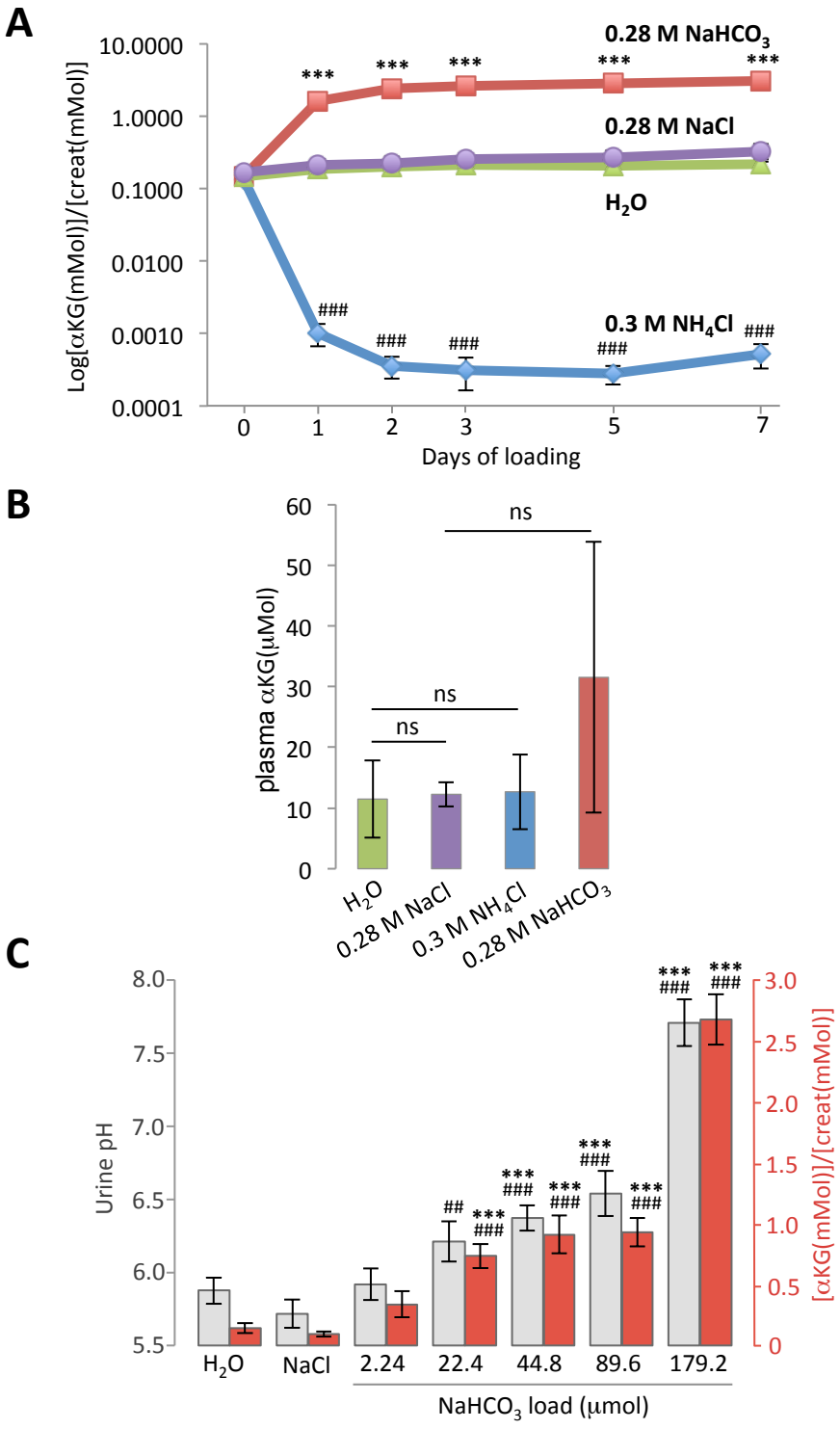

Figure 3. Tokonami et al.

Table 1. Blood and urine chemistry in wild-type and oxgr1-/- mice

Standard Diet

Blood/plasma	**wild-type**	**oxgr1-/-**	**p**
Na^+ (mM)	151.8 ± 3.1 (7)	146.1 ± 1.6 (7)	NS
K^+ (mM)	4.6 ± 0.2 (7)	4.6 ± 0.1 (7)	NS
Cl^- (mM)	118.7 ± 2.0 (10)	116.9 ± 2.4 (10)	NS
HCO_3^- (mM)	22.6 ± 0.4 (10)	22.8 ± 0.5 (10)	NS
pCO_2 (mmHg)	45.0 ± 4.2 (10)	38.6 ± 1.4 (10)	NS
pO_2 (mmHg)	128.0 ± 10 (10)	127.5 ± 7.0 (10)	NS
pH	7.35 ± 0.02 (10)	7.39 ± 0.02 (10)	NS
Osmolality (mOsm)	325.6 ± 4.6 (5)	324.3 ± 1.2 (7)	NS
aldosterone (pg/ml)	337.5 ± 36.9 (11)	380.5 ± 26.1.2 (10)	NS
Urine			
Na^+/creatinine (mmol/mmol)	11.9 ± 0.4 (32)	12.0 ± 0.5 (33)	NS
K^+/creatinine (mmol/mmol)	52.7 ± 1.5 (32)	57.4 ± 2.5 (33)	NS
Cl^-/creatinine (mmol/mmol)	20.1 ± 1.1 (23)	22.7 ± 1.4 (25)	NS
TA/creatinine (mmol/mmol)	6.1 ± 0.4 (23)	8.0 ± 0.6 (25)	0.008
NH_4^+/creatinine (mmol/mmol)	11.8 ± 1.1 (23)	12.6 ± 1.4 (25)	NS
αKG/creatinine (mmol/mmol)	0.11 ± 0.01 (23)	0.14 ± 0.01 (25)	0.03
pH	6.24 ± 0.02 (32)	6.10 ± 0.02 (33)	0.00001
Volume (ml/24 h)	1.36 ± 0.07 (32)	1.41 ± 0.07 (33)	NS
Base-rich diet (3 days)			
Blood/plasma			
Na^+ (mM)	147.9 ± 0.6 (10)	147.9 ± 1.0 (10)	NS
Cl^- (mM)	113.7 ± 0.7 (10)	112.0 ± 1.0 (10)	0.0004
HCO_3^- (mM)	30.6 ± 1.5 (10)	33.4 ± 2.89 (10)	0.01
pH	7.38 ± 0.06 (10)	7.39 ± 0.04 (10)	NS
Urine			
Na^+/creatinine (mmol/mmol)	57.1 ± 3.6 (6)	53.2 ± 9.3 (6)	NS
K^+/creatinine (mmol/mmol)	14.0 ± 1.1 (6)	13.3 ± 3.0 (6)	NS
Cl^-/creatinine (mmol/mmol)	9.9 ± 0.5 (6)	9.2 ± 2.1 (6)	NS
pH	9.00 ± 0.11 (6)	8.95 ± 0.17 (6)	NS
Volume (ml/24 h)	4.84 ± 0.40 (6)	5.23 ± 1.47 (6)	NS
FE_{HCO3}(%)	3.5 ± 1.4 (5)	1.5 ± 0.5 (5)	0.017

Values are means ± SD. Student's t-test.
All urine and blood samples were collected from independent mice.

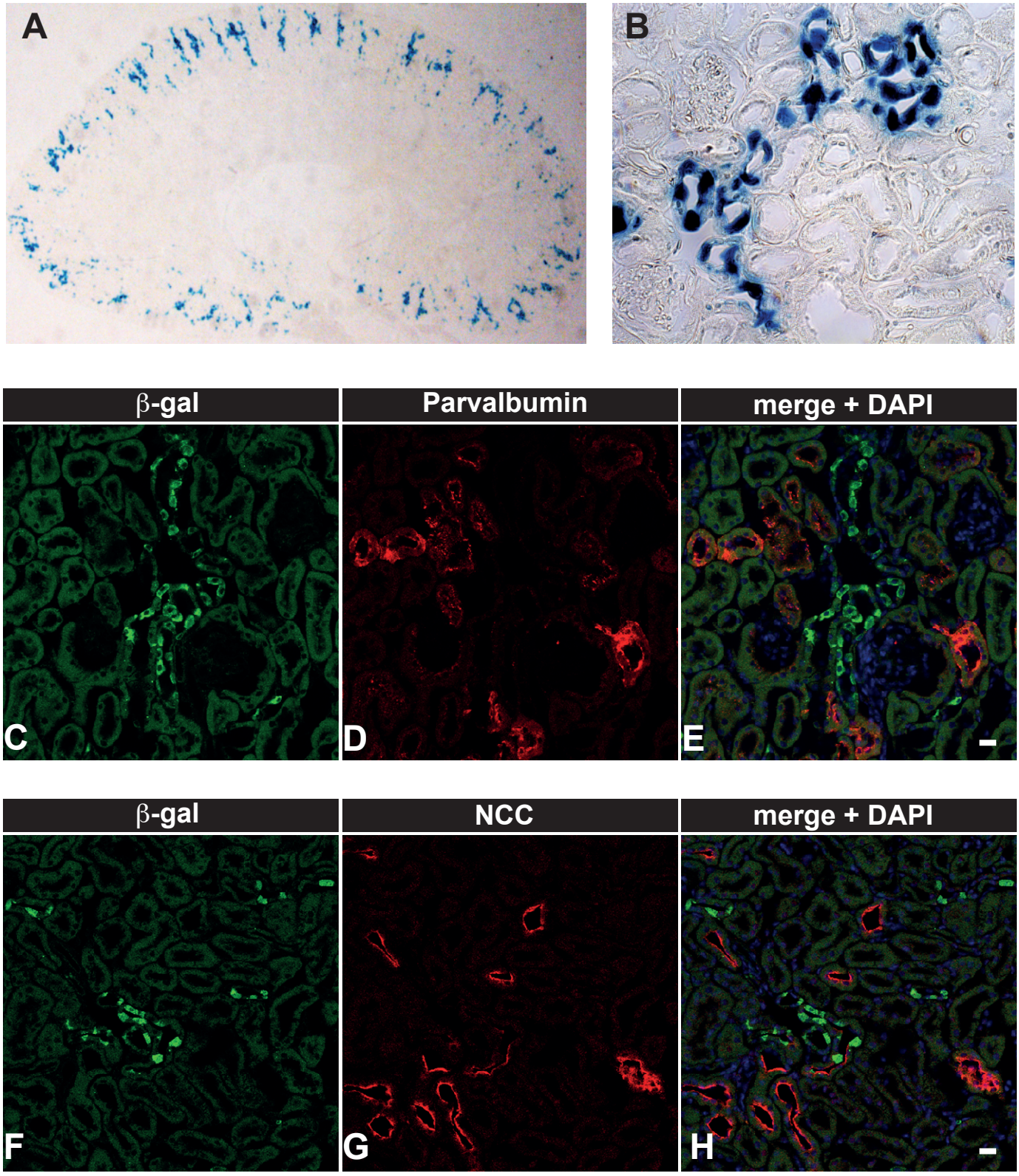

Supplementary Figure 1 (A-H). Oxgr1 expression in the kidney. **A**. Low magnification image of X-gal (Oxgr1) staining on frozen kidney section. This image demonstrates that Oxgr1 expression is limited to the renal cortex. **B**. High magnification image of (A) - demonstrates patchy distribution of Oxgr1-positive cells along the cortical nephron. **C** and **F**. Immunostaining with an antibody against β-galactosidase (green) confirms the patchy expression of Oxgr1 in the renal cortex. **D** and **G**. Immunostainig of two specific markers for the initial part of the distal convoluted tubule (DCT1), parvalbumin and the sodium-chloride cotransporter (NCC), respectively. **E** and **H**. Co-immunostaining of Oxgr1 with parvalbumin or NCC, respectively, demonstrates that Oxgr1 is not expressed in the DCT1. Scale bars: 50 μm.

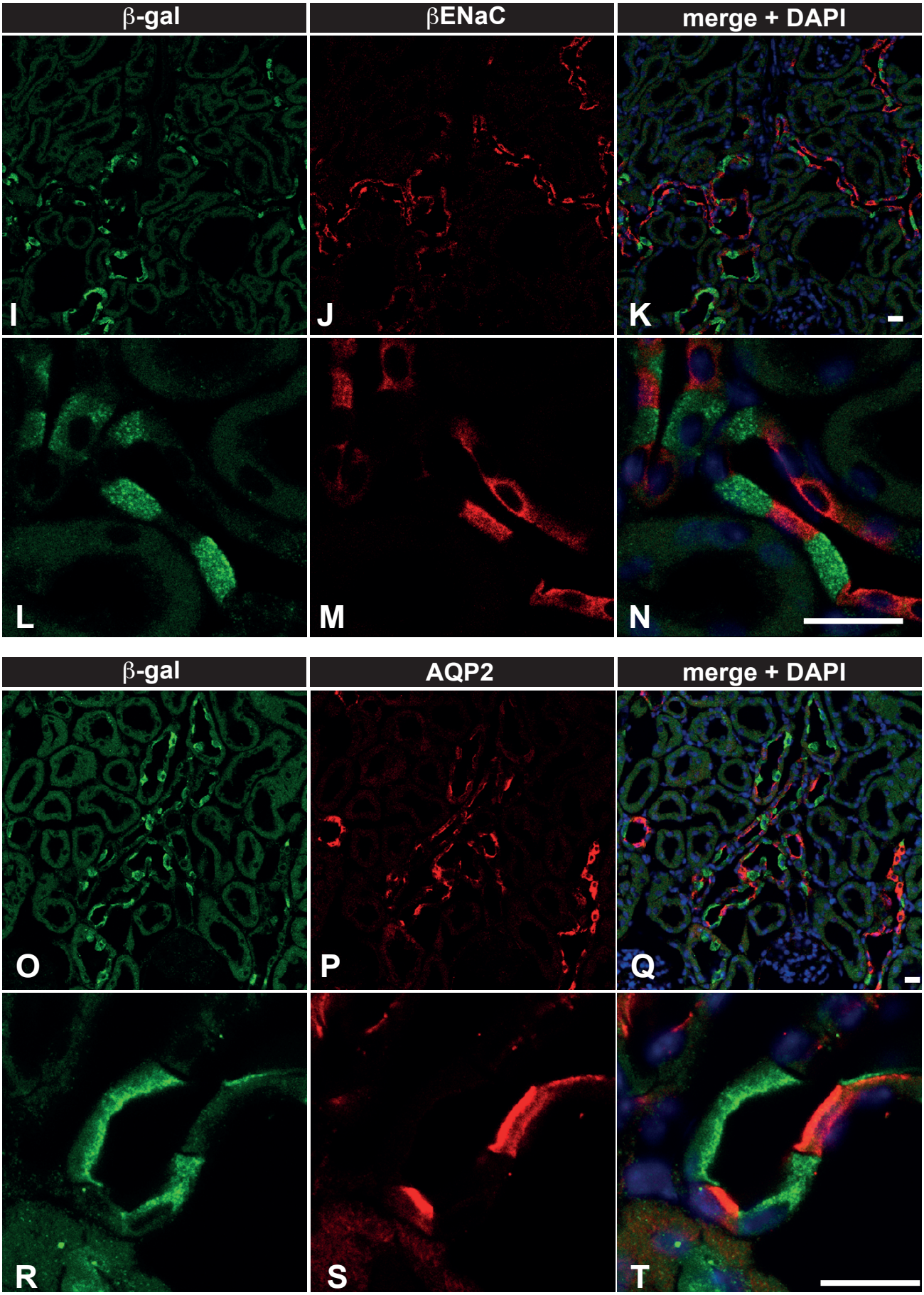

Supplementary Figure 1 (I-T). **Oxgr1 expression in the kidney.** **I** and **O**. Immunostaining with an antibody against β-galactosidase (green) in the renal cortex. This staining reveals patchy distribution of Oxgr1 in the cortical segments of the collecting system. **J** and **P**. Immunostaining of two specific markers for principal cells in the CNT and the CCD, beta subunit of the epithelial sodium channel (βENaC, red) and the aquaporin-2 water channel (AQP2, red), respectively. **K** and **Q**. Co-immunostaining of Oxgr1 with βENaC or AQP2, respectively, demonstrates that Oxgr1 is expressed in the same tubular segments, but not in principal cells. **L**, **M**, **N**, **R**, **S** and **T** are high magnification images of I, J, K, R, S and T, respectively. Scale bars: 50 μm.

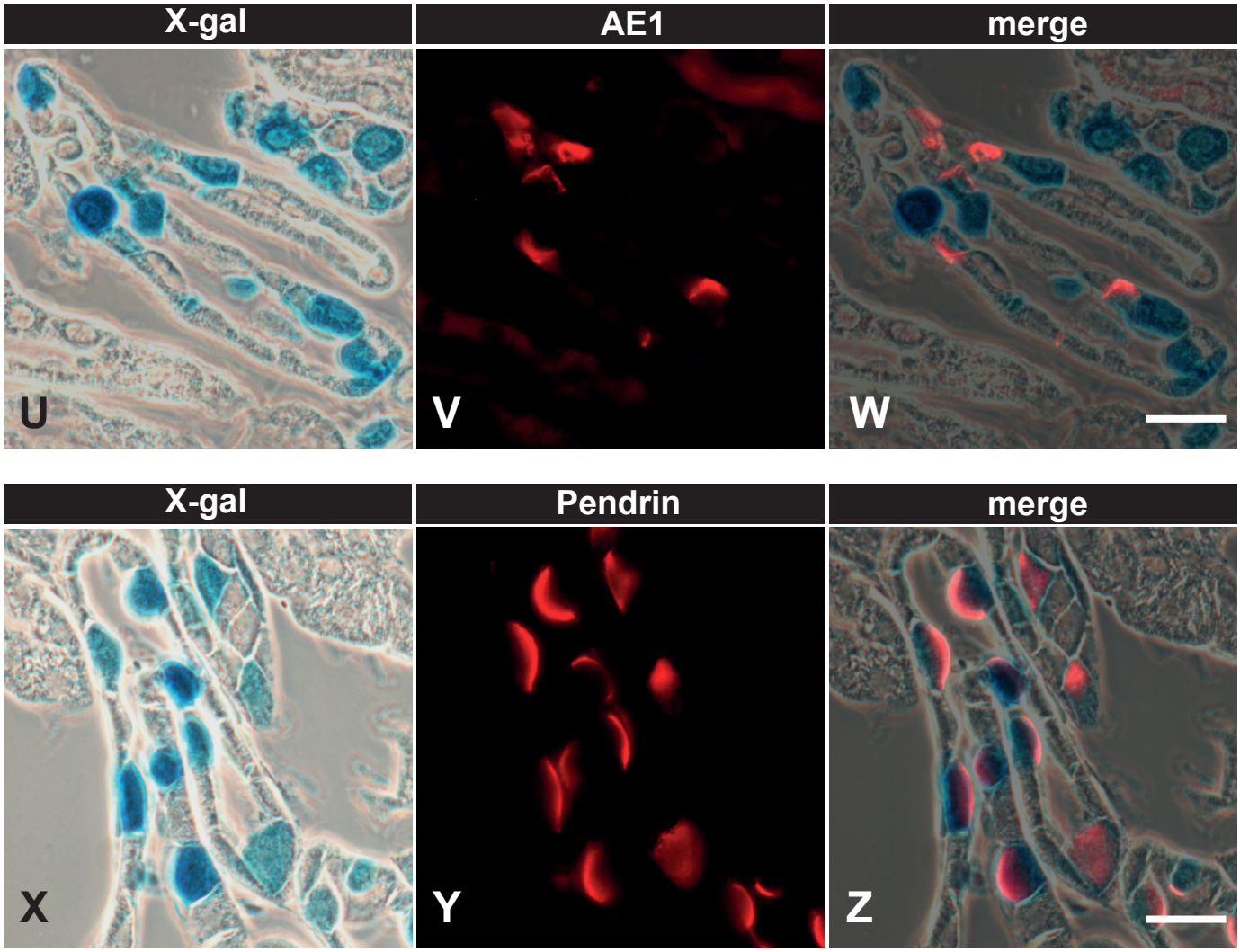

Supplementary Figure 1 (U-Z). Oxgr1 expression in the kidney. **U** and **X.** Oxgr1 (X-gal) staining (blue) in the renal cortex. **V**. Immunostaining of anion exchanger 1 (AE1, red) in the basolateral membrane of type-A intercalated cells. **W**. Co-staining of Oxgr1 and AE1 shows that Oxgr1 is expressed in the same tubular segments, but not in type-A intercalated cells. **Y**. Immunostaining of pendrin (red) in the apical membrane of type-B and non-A-non-B intercalated cells. **Z**. Co-staining of Oxgr1 with pendrin confirms that Oxgr1 is expressed in type-B and non-A-non-B intercalated cells. The Oxgr1(Xgal)/pendrin(Ab) co-staining also demonstrates that X-gal staining does not interfere with immunohistochemistry. Scale bars: 50 μm

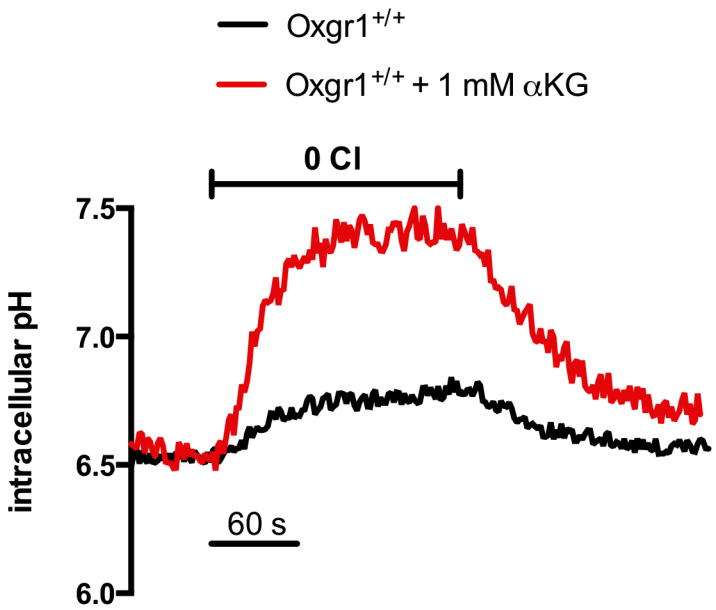

Supplementary Figure 2. Representative traces of the changes in pHi elicited by luminal Cl^- removal and then re-addition, in the presence of extracellular HCO_3^- (25mM, pH 7.40) and in Na^+-free solutions. The traces have been recorded on 2 distinct tubules from $Oxgr1^{+/+}$ mice, in the absence (black trace) and in the presence (red trace) of 1 mM alpha-keto-glutarate in the lumen.

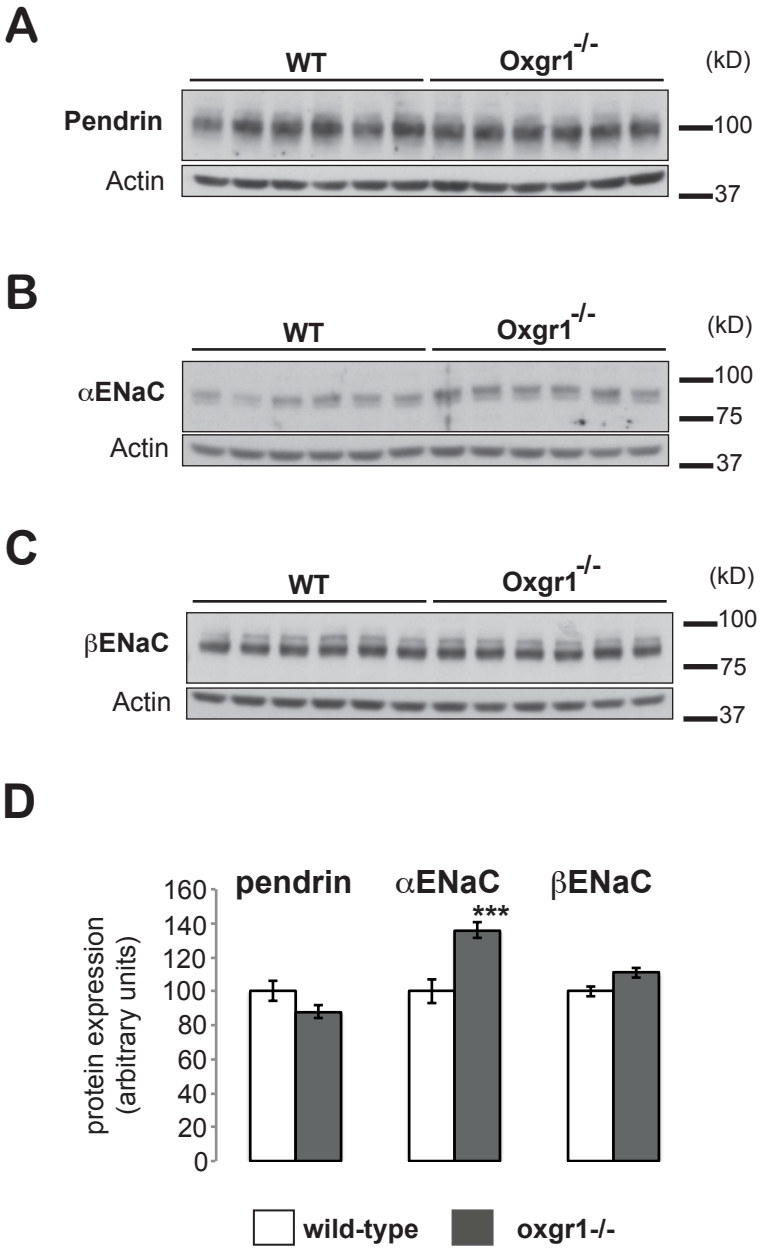

Supplementary Figure 3. Pendrin (**A**), αENaC (**B**) and βENaC (**C**) protein abundance in kidneys of wild-type and oxgr1**-/-** mice. Western blots were performed as described in Supplementary Methods. Acting was used as the loading control. (**D**) Densitometric quantitaion of Wester blot data presented in panels A, B and C. Values are means ± SEM. *** - significantly different compared to wild-type mice. Student's t-test.

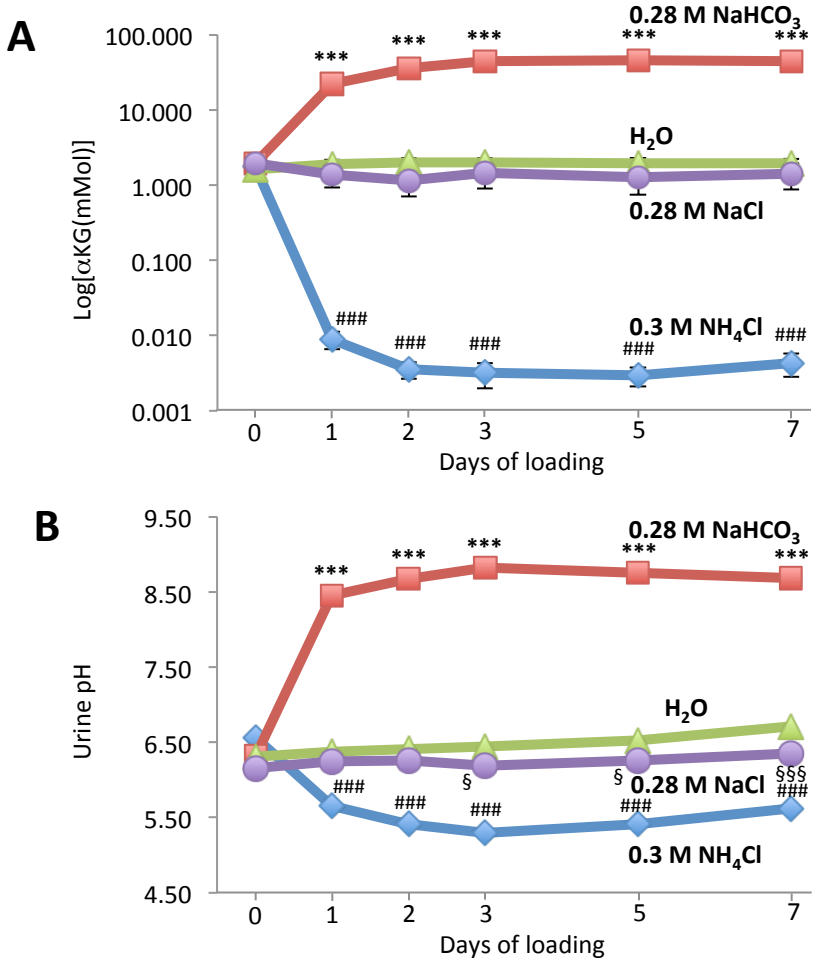

Supplementary Figure 4. Effects of a dietary load of acid, base or NaCl on (**A**) urinary concentration of αKG, and (**B**) urine pH. These parameters were tested in urines collected from wild-type mice housed individually in metabolic cages. The 24-hour urine was collected from four groups of mice (6 mice/group): a control group receiving tap-water (green) and groups supplemented with acid (0.3 M NH_4Cl, blue), alkali (0.28 M $NaHCO_3$, red) or salt (0.28 M NaCl, purple) in drinking water. Values are means ± SEM. *, significantly different (*, $P<0.05$; **, $P<0.01$; ***, $P<0.005$) compared to 0.28 M NaCl group; #, significantly different (###, $P<0.005$) compared to H_2O group; §, significantly different (§, $P<0.05$; §§§, $P<0.005$) compared to H_2O group; Student's t-test.

Supplementary Figure 5. Role of αKG/Oxgr1 intra-renal paracrine mechanism in maintaining the acid-base equilibrium.

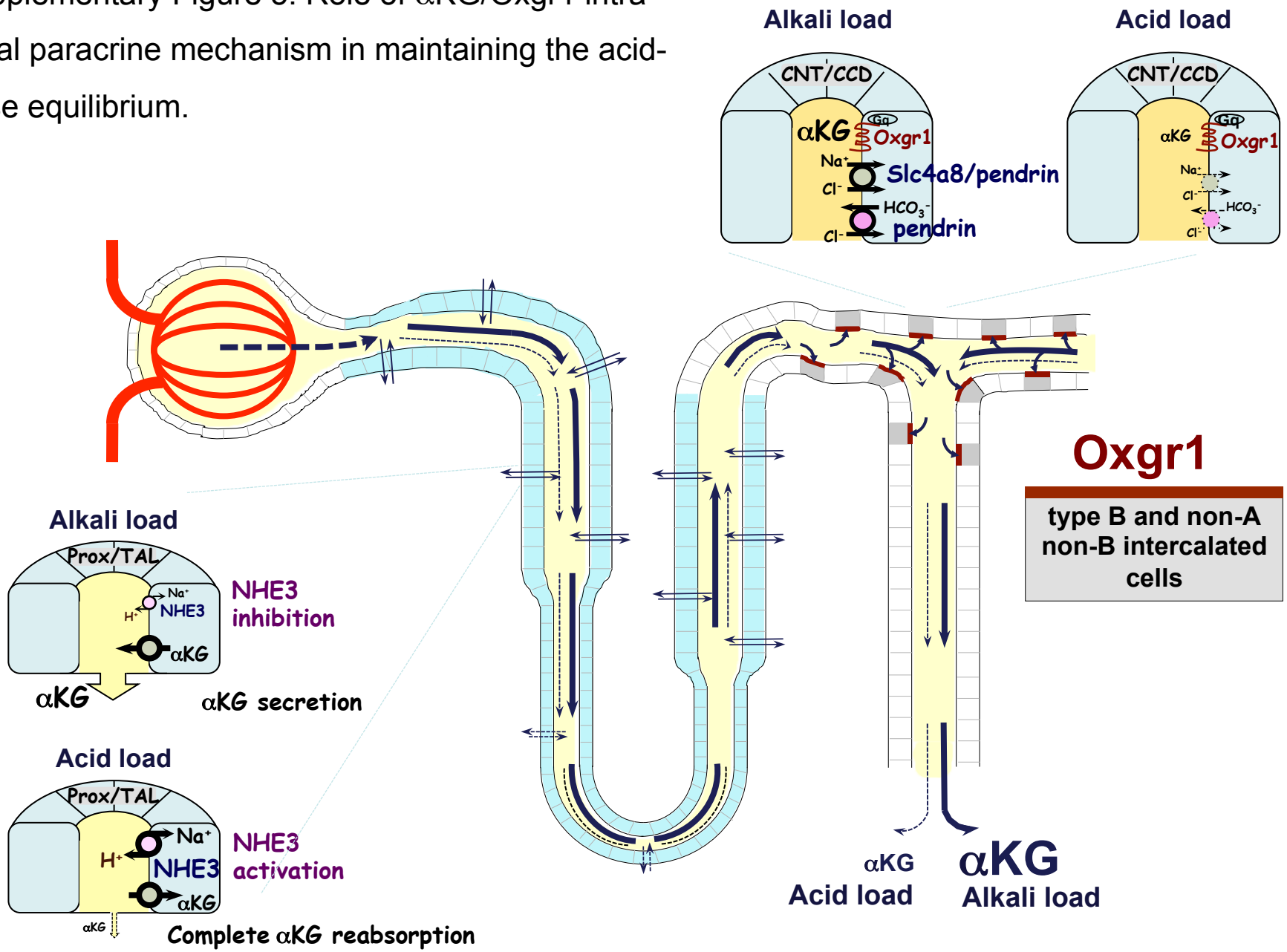

Supplementary Methods.

Identification of type B and non-A-non-B intercalated cells for pHi measurement.

Intercalated cells were identified by apical labeling with fluorescent peanut lectin (PNA, Vector Labs). Apical PNA labeling does not allow for discrimination between the different subtypes of intercalated cells. The type A cells were excluded from analysis on the basis of their bigger size and the lack of luminal Cl^--dependent change in intracellular pH. According to these criteria, approximately 55-65% of intercalated cells were classified as type A. Because BCECF was loaded from the peritubular fluid, the principal cells also displayed a significant fluorescence at the end of the BCECF exposure. They were excluded from the analysis on the basis of (i) the absence of PNA labeling and (ii) the lack of luminal Cl^--dependent change in intracellular pH. Use of fluorescein-coupled PNA allowed using the same set of filters for identification of cell types and pH measurements. However, PNA fluorescence did not interfere with BCECF fluorescence because it is restricted to the apical membrane and not the cytosol, and a much higher intensity of the excitation light was required to see the PNA fluorescence than the pH-sensitive BCECF fluorescence. Thus, after the cells labeled with PNA were identified, the illumination intensity was decreased and set to the BCECF requirements.

X-gal staining and Immunohistochemistry. Mice were anesthetized with ketamine/ xylazine and kidneys were perfused from the renal artery with 20 ml of 2% paraformaldehyde/PBS, then transferred to 30% sucrose/PBS and embedded to O.C.T. compound (Tissue-Tek). X-gal staining and immunostaining were performed on 8 μm-thick cryostat sections. For the X-gal staining, sections were incubated in the staining solution containing 5mM $K_3Fe(CN)_6$, 5mM $K_4Fe(CN)_6$, 2mM $MgCl_2$, 0.05% Tween-

20 in PBS followed by overnight incubation in the same staining solution to which the X-gal was added (1mg/ml, Invitrogen) (RT). Sections were washed with PBS, dehydrated and mounted in Roti-histokitt (Roth). For the immunostaining, sections were blocked with 10% normal donkey serum (Millipore), 0.05% Tween-20 in PBS, then incubated with primary antibody diluted in the blocking solution. After washing steps, sections were incubated with the secondary antibody: anti-rabbit alexa555 conjugated IgG or anti-chicken alexa488 conjugated IgG (Invitrogen) for 2 hours followed by the incubation with DAPI for nucleus staining. Immunostained sections were mounted in ProLong Gold antifade reagent (Invitrogen). For the double staining of X-gal and AE1, first, sections were stained with X-gal as described above. Then, the antigen-retrieval treatment was performed for AE1. Sections were microwaved for 15 minutes in the solution containing 10mM Na-citrate and 1mM EDTA and were cooled down at the room temperature. After washing steps, immunostaining was performed as described above. For double staining of X-gal and pendrin, the immunostaining (pendrin) was performed without antigen-retrieval. Images of X-gal staining, double immunofluorescence staining, and double staining of X-gal and immunofluorescence were obtained by stereomicroscope MZ16FA (Leica), confocal microscope SP5 (Leica) and Axovision (Zeiss) respectively. All images were processed with Adobe Photoshop (Adobe).

Western blotting Whole decapsulated kidneys (6 mice per genotype) were homogenized with a polytron in 3 ml RIPA buffer containing 50mM Tris-HCl (pH 7.2), 150mM NaCl, 0.1% SDS, 0.5% Na-deoxycholate, 1% NP40, 1mM PMSF and protease inhibitors. Protein extracts were sonicated and centrifuged for 5 minute at 1500rpm. The supernatant was recovered and the protein concentration was measured with Pierce BCA protein assay reagent (Thermo), then the concentration was adjusted

to 8mg/ml with RIPA buffer. Samples were mixed with Laemmli sample buffer (BIO-RAD) supplemented with 2-mercaptoethanol (SIGMA), and were heated for 15 minutes at 56 degrees C. 40μg of protein samples were migrated in the Mini-PROTEAN TGX gels, 4-20% (BIO-RAD), then transferred to the nitrocellulose membrane in the transfer buffer containing 20% Methanol. Membranes were stained with Ponseau S and then washed in TBS containing 0.2% NP40. Then, membranes were incubated with 5% skim milk in 0.2% NP40/TBS for 1 hour at the room temperature for the blocking, followed by the incubation with primary antibodies in the blocking solution, overnight (cold room). Membranes were washed and blocked as above, and incubated with anti-rabbit horseradish peroxidase conjugated IgG in 5% skim milk in 0.2% NP40/TBS for 1 hour at the room temperature. After the washing steps, SuperSignal west dura extended duration substrate (Thermo) was used and signals were visualized on Kodak Biomax XAR film (Kodak). Bands were digitalized by Epson Expression 1680 (EPSON) and were quantified with Quantity One 1-D Analysis software (BIO-RAD).